Characterization of interdiffusion around miscibility gap of lattice matched InGaAs/InP quantum wells by high resolution x-ray diffraction

F. Bollet
MATAR, London College of Communication, University of the Arts London, Elephant and Castle, London SE1 6SB, United Kingdom

W. P. Gillin[a)]
Department of Physics, Queen Mary, University of London, Mile End Road, London E1 4NS, United Kingdom

(Received 18 September 2006; accepted 23 October 2006; published online 3 January 2007)

A methodology to characterize of thermally interdiffused heterostructures by high resolution x-ray diffraction is presented. The technique provides detailed information on the strains and compositions generated throughout the interdiffusion process in a 10 nm lattice matched InGaAs/InP sample annealed at 800 °C. It shows that the diffusion process is complex and subject to the influence of the miscibility gap in the quaternary InGaAsP system. The technique also appears to provide a route to mapping the binodal isotherms of the InGaAsP miscibility gap. © *2007 American Institute of Physics*. [DOI: 10.1063/1.2404784]

I. INTRODUCTION

A. Coherency strains and mechanical strengthening

Coherently strained thin layers are a known source of strengthening mechanisms for structural materials. For example, coherent or semicoherent lamellar structures developed by spinodal decomposition within the grains of polycrystalline alloys, such as copper-nickel or titanium-aluminum, can dramatically improve their high temperature mechanical properties.[1] Grain size and lamellar periodicity are important parameters for these materials.[2] In large coherently strained pseudomorphic crystals, such as semiconductor superlattice structures, the alternation of ultrathin layers in tension and compression is also seen to improve structural properties at both high[3] and room[4] temperatures. There are no grain boundaries in these crystals, and there is a degree of control on the generation and propagation of the dislocations responsible for single crystal deformation, solely by virtue of the alternating strain field.

By providing nearly defect free single crystals and offering accurate, but also flexible compositions at any point of the growth, epitaxial technology could potentially produce large multilayer pseudomorphic structures, with remarkable properties, that alternate coherency strains of opposite signs. Those properties could also be tailored for the desired requirements of the material at low or high temperatures by varying parameters such as strain modulation and wavelength of the repeat layers. In the long term it offers the possibility to manufacture macroscopic flawless objects with observable mechanical properties comparable to their interatomic bond strengths.

The road is nevertheless still a long one, as current epitaxial growth technologies are notoriously very slow and expensive. Also, the modulated strain field in these superlattices is commensurate to the modulated composition of the layered crystal, thus making the structure unstable to atomic diffusion at high temperatures along compositional gradients. As mentioned earlier, metal alloys sometime generate, by spinodal decomposition, grains with a coherent layered structure that remains thermodynamically stable at high temperature. In a similar manner, it might be possible to prevent the homogenization of epitaxially grown superlattices by selecting materials with a positive enthalpy of mixing.

B. Characterization of diffusion

With the considerable potential of coherently strained thin-layered materials, the need to ascertain their durability against high temperature diffusion requires further understanding. The current semiconductor technology of molecular beam epitaxy (MBE) is perfect for manufacturing accurate and reliable model crystals to investigate either the strengthening mechanisms in superlattices or atomic diffusion and intermixing. Diffusion in pseudomorphic crystals forming quantum well (QW) structures has long been characterized using photouminescence (PL), which monitors well barrier interdiffusion by measuring the alteration of the QW light emission wavelength. InGaAs/InP heterostructures are routinely grown by MBE, and the InGaAsP system presents a miscibility gap. It is therefore an ideal system to investigate the impact of a miscibility gap on the interdiffusion process.

Nevertheless, the interpretation of PL experiments has relied on various assumptions, such as a model for the interdiffusion of the heterostructure to relate a given PL energy shift to a state of diffusion. Previous studies, that also used high resolution x-ray diffraction (HRXRD) as a tool of characterization of diffusion, showed that a model such as Fick's laws with a constant coefficient of diffusion could not be taken for granted for lattice matched InGaAs/InP heterostructures.[5,6] And indeed, another study on the *a priori* straightforward InGaAs/GaAs system clearly showed that indium is not a simple marker of diffusion, and that diffusion cannot be modeled with Fick's laws and a constant coeffi-

[a)]Electronic mail: w.gillin@qmul.ac.uk

cient of diffusion.[7] Hence, the latter model is highly unlikely to be suitable at all to the InGaAs/InP system, which is further complicated by interdiffusion on two sublattices (of group III and V atoms) and the presence of a miscibility gap in the InGaAsP quaternary diagram.

The present study uses the wealth of information contained in HRXRD experimental rocking curves of diffused InGaAs/InP QW specimens to quantitatively characterize the strains and compositions formed during interdiffusion. Beyond the structural materials and strengthening mechanism context, the understanding of interdiffusion is also of interest for the fabrication of semiconductor devices.

C. Miscibility gap

The miscibility gap in the InGaAsP system was predicted by De Cremoux *et al.*,[8] who also calculated its contours for several temperatures. The calculations were later refined by Stringfellow[9] and Onabe[10] who used different methods of calculation but obtained qualitatively similar results. Figure 9 displays a representation of the miscibility gap in the InGaAsP quaternary diagram that is inspired from Stringfellow's publications. Stringfellow calculated the critical temperature below which the miscibility would appear and determined a value of 1081 K. But there is often a discrepancy between the calculated diagrams and critical temperatures, and their experimental confirmations, even in the case of simple binary systems. It is also important to note that the diagrams usually presented do not take strains into account. Coherently strained layers appear to have a much higher resistance to decomposition, and critical temperatures can be greatly lowered in the case of a coherent phase grown on a substrate with a lattice mismatch.[11] This point is illustrated by Schlenker *et al.*,[12] who published detailed calculated contours of immiscibility for some III-V quaternary systems. These contours show the expected effect of strains for pseudomorphic alloy layers grown on a substrate.

Currently, there are no thorough experimental measurements of the critical temperature, strain effects, and limits of the miscibility gap at a given temperature for the InGaAsP system. The information is nevertheless important for the growth quality of crystals, their electronic properties, and their resilience to conditions of utilization in devices. Crystals have been grown with compositions within the miscibility gap, especially using nonequilibrium growth methods. But the questions of in-grown defects and stability with time and temperature are still important.

II. EXPERIMENTAL METHOD

A. Sample and general procedure

A 10 nm $In_{0.53}Ga_{0.47}As$ single quantum well (SQW) sample, lattice matched to 001 InP substrates, was grown by MBE. It consisted of an InP buffer layer (~300 nm), the quantum well, and a 100 nm InP barrier layer. A 50 nm silicon nitride capping layer was subsequently deposited by plasma enhanced chemical vapor deposition to prevent surface decomposition during annealing.

The sample annealed was about 7×5 mm^2, and a detailed HRXRD characterization of the as-grown material has already been conducted in a previous publication.[6]

The sample was subjected to a rapid thermal annealing (RTA) in a helium ambient using a triple graphite strip heater with the temperature controlled by an Accufibre optical thermometry system. The system was calibrated against the melting point of silver and was found to be accurate to ±1 °C. Anneals of various durations were performed at 800 °C and the SQW diffusion was characterized by HRXRD and low temperature (80 K) PL measurements.

B. HRXRD

1. Rocking curves

For an infinite perfect crystal and perfect experimental conditions, diffraction spots are delta functions of intensity. For an ultrathin crystal along a given crystallographic direction, all diffraction spots become elongated in the corresponding reciprocal direction. Diffracted x rays carry information about the diffracting planes, but they also carry information about the whole volume of specimen probed, and each Laue spot is the delta function mention above, corrected for imperfections and crystalline domain size limits, and convolved with a Fourier transform of the macroscopic structure of the crystal.[13] It follows that layers of different compositions and different indices of refraction in a pseudomorphic crystal will give rise to a modulation of the Laue spot intensity and generate fringe characteristic of the geometrical transform of the crystal. HRXRD is a technique that provides a high angular resolution and allows measurement of intensity profiles across the Laue spots by rocking the specimen through its Bragg angle; these intensity profiles are called rocking curves. The technique requires a low angular divergence and low spectral dispersion of the incident x-ray beam, and high stepping accuracy of diffractometer's goniometer. Figure 1 displays simulations of 002 and 004 rocking curves for the nominal QW structure described in Sec. II. The high frequency fringes are characteristic of the 100 nm top barrier layer that is decoupled from the bulk substrate by the QW layer, but the fringes cannot be fitted or information cannot be extracted from them without considering the quantum well layer, which in this case does not have a negligible thickness.[14] These fringes evolve from a more complex situation than equal thickness fringes observed in the simple Fraunhofer case in reflectivity measurements.

2. Modeling

Although in theory, macroscopic structural information about the heterostructures and layer thickness could be worked out backward with direct measurements of the various fringes angular spacing in experimental rocking curve; in practice the diffraction process is complex. For example, in the case of a near perfect crystal with a thin layer on a substrate and a long x-ray coherent length, the specimen volume coherently probed embraces the layer and substrate. The layer cannot be treated independent of the substrate and more generally of any other neighboring layers. Experimentally, the peak position of a strained layer can be seen to differ for

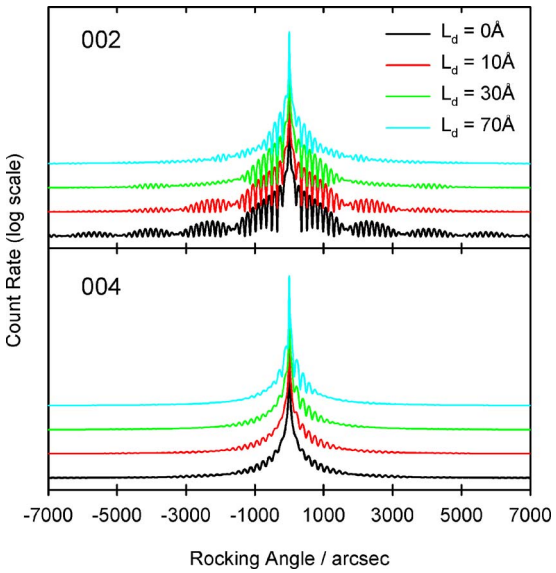

FIG. 1. (Color online) Rocking curve simulations showing the effect of interdiffusion in a 10 nm lattice matched InGaAs/InP QW structure when group III and V atoms interdiffuse at the same rate. The Fickian model with a constant coefficient of diffusion was used. The 004 rocking curves show a slight increase and persistence of some fringes caused by the small tensile strains generated by a departure from Vegard's law in the InGaAsP system.

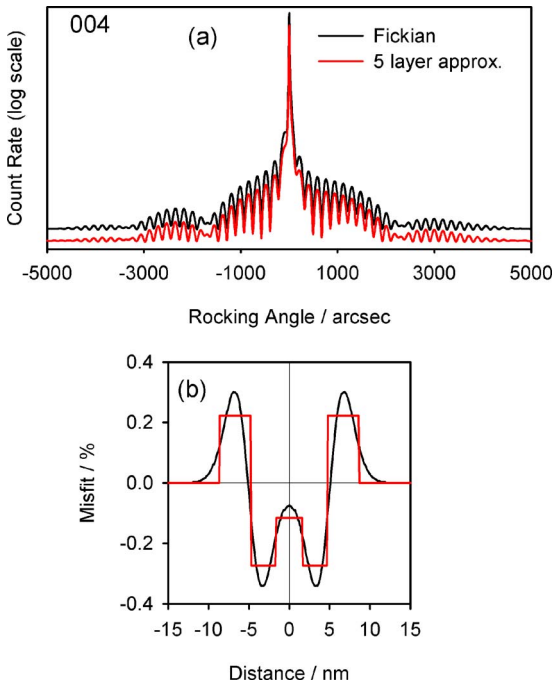

FIG. 2. (Color online) Rocking curve simulations showing the effect of diffusion with different rates for group III and V atoms in a 10 nm lattice matched InGaAs/InP QW structure. Here, diffusion follows Fick's model with constant, but different coefficient of diffusion for group III and V atoms, with $L_{d\mathrm{III}}=20$ Å and $L_{d\mathrm{V}}=30$ Å. The resulting strains generate strong fringe amplifications on the 004 rocking curve profile. The rocking curve can be reproduced with a simple five homogeneously strained layer model, thus opening a possibility of simple curve fitting of experimental measurements. (a) shows an accurate curve fit of the 004 rocking curve, and (b) shows the approximation made by the curve fitting routine on a strain diagram. Only strains, not compositions, were used to fit the 004 curve.

layers of identical composition, but different thickness. The layer feature appears to be pulled closer to the neighboring intense substrate peak with decreasing layer thickness. Information is best extracted by modeling the diffraction process with the dynamical theory of diffraction that takes into account the x-ray beam extinction with depth and the infinite multiplicity of forward and backward scatterings by atomic planes to evaluate the complete wave field inside the heterostructure.[15] The kinematical model that makes use of simpler calculations with plane waves and single scattering events can also be used, providing that individual layers interact weakly with the x-ray beam and that contributions from multiple scattering can be ignored.[16] For the purpose of this study, complete rocking curve simulations can be calculated using the dynamical theory of diffraction with Philips X'PERT EPITAXY 3.0 software package. The software calculates theoretical rocking curve from virtual pseudomorphic crystals constituted of layers of uniform compositions. SMOOTHFIT, a companion software, allows some curve fitting of experimental curves from close virtual models by tuning the structural parameters (layer composition and thickness). Further explanations and details of the kinematical and dynamical theories of diffraction can be found in the literature.[13]

Figure 1 shows simulated 002 and 004 rocking curves for a nominal specimen (i.e., a 10 nm lattice matched InGaAs/InP QW) that would have diffused according to Fick's laws with a constant and identical coefficient of diffusion for group III and V atoms. Rocking curves for several diffusion lengths are presented. With the progress of diffusion, fringe intensity is seen to diminish. In the extreme case of a complete homogenization of the structure, they would disappear completely. Note that 004 rocking curves are very sensitive to strains, and that very small tensile strains are picked up. These strains arise during diffusion from the slight bowing of the isostrain lines in the quaternary diagram and are at the most of the order of 0.03%. They are sufficient to enhance slightly the first fringes on the tensile side of the substrate peak and to allow the fringes to persist for significant diffusion lengths.

Should diffusion rates be different for group III and V atoms, significant strains are generated. Figure 2(a) shows a simulated 004 rocking curve for a nominal specimen that would have a higher group V atom diffusion rate. In this case, diffusion would have followed Fick's laws with constant coefficients of diffusion and the diffusion lengths for group III and V atoms would be, respectively, 2 and 3 nm. Large fringe amplifications modulated by the strained domain sizes are clearly visible on the 004 profile. The corresponding strain profile is presented in Fig. 2(b).

3. Simple rocking curve fit

In order to have a stable fit to experimental curves with the SMOOTHFIT software, the virtual model structure used to calculate and adjust the fitting curves should be as simple as possible, while retaining sufficient complexity to meaningfully describe the actual strains measured. The simulations in Fig. 1 and 2 were generated by calculations on virtual structures containing over 40 layers of constant composition that were closely matching composition distributions calculated with error functions. It is not possible to enter such a com-

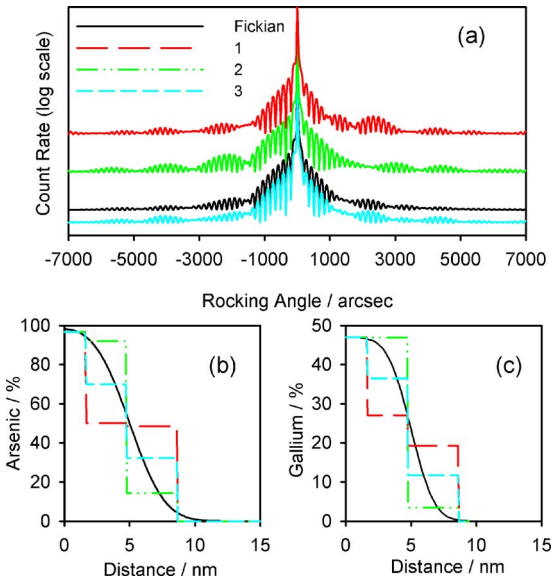

FIG. 3. (Color online) The fit of Fig. 2 is refined by a compositional fit made on the 002 rocking curve of the simulated strained structure of Fig. 2. Results of the strain fit of Fig. 2(b) are conserved, and compositions of the five layers are adjusted to fit the 002 profile. Three possible fits with identical strain fields are presented in (b) and (c), and their calculated 002 rocking curves shown in (a). Clearly solution 3 provides the closest 002 fit in (a), and the best approximation to the actual composition profile (thick black line) in (b) and (c).

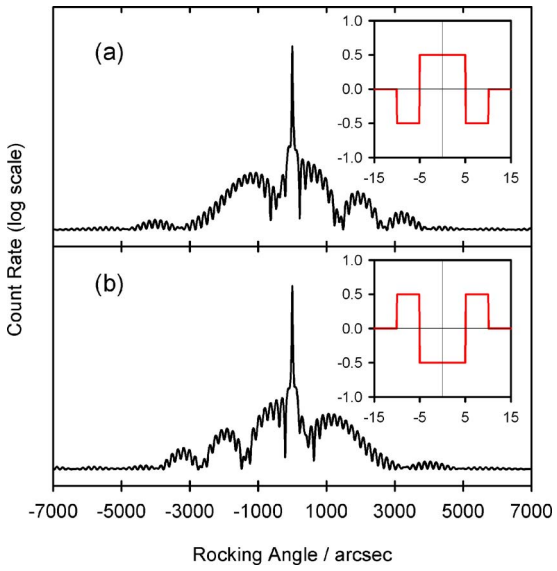

FIG. 4. (Color online) Qualitative description of 004 rocking curves when group III atoms (a) or group V atoms (b) interdiffuse at a higher rate. The misfit strain (%) against depth profiles used to generate the 004 rocking curves is also shown (insets).

plex structure and to let the SMOOTHFIT software freely adjust parameters to fit experimental rocking curves. The fitting procedure was rationalized by approximately fitting strains detected on 004 experimental profiles with four or five homogeneous layers symmetric with regard to the QW center, and then refining composition distributions by fitting the corresponding 002 experimental rocking curves. Figure 2(a) shows that it is possible to fit closely the 004 profile of a complex structure with the simpler strain profile in Fig. 2(b). As seen in the latter, a simple five-layer structure provides an accurate description of the magnitude and location of the strain field. To obtain further information on actual compositions, the layer strain and thickness values deduced from 004-profile fits are conserved and reused to fit the corresponding 002 profiles. By using a spreadsheet software and imposing conditions such as layer thickness, layer strain, and total quantities of gallium and arsenic in the specimen, it is possible to calculate the range of possible layer composition. By a process of trial and error, a composition approximation is made by comparing calculated 002 profiles with the experimental data. Figure 3 shows several possible composition profiles that have identical strain distributions and their corresponding 002 rocking curves. Clearly, rocking curve 3 provides the closest fit and an accurate description of the actual composition profile.

This procedure is used to model actual experimental data and extract information on strains and compositions of diffused experimental samples. As already mentioned, unequal rates of diffusion on group III and V sublattices generate strains in the crystal that are easily picked up by 004 rocking curve measurements. The 004 experimental measurements should qualitatively appear as in Fig. 4, where the two possibilities, larger diffusion rate for group III or V, are illustrated.

III. RESULTS AND DISCUSSION

Figure 5 shows PL shifts as a function of anneal time at 800 °C, with an initial blueshift of the photoluminescence, followed by a relative red shift. The corresponding 004 rocking curve measurements are presented in Fig. 6. Strains are clearly observed throughout the diffusion process. By referring to Fig. 4, the initially unstrained specimen can be seen to have developed tensile strains in the well layer and compressive strains in the barrier layers following annealing for up to 2400 s (40 min).

This is consistent with a higher rate of diffusion of group V atoms.[5] The corresponding PL data in Fig. 5 show a monotonic blueshift up to 2400 s (40 min) into the annealing. At

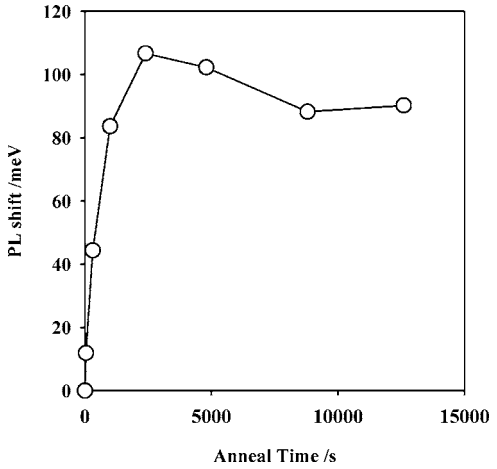

FIG. 5. Experimental PL shifts as a function of anneal time at 800 °C of 10 nm lattice matched InGaAs/InP QW heterostructure.

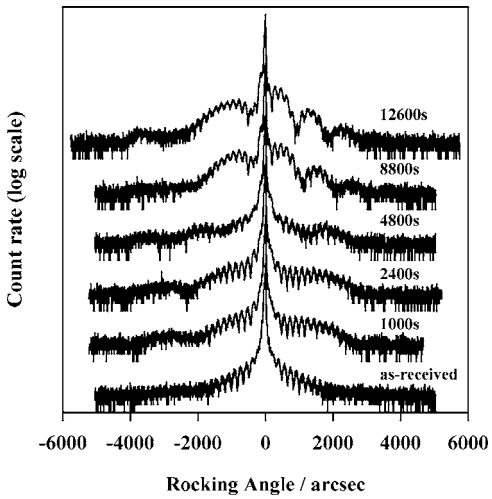

FIG. 6. Experimental 004 rocking curves of a 10 nm lattice matched InGaAs/InP QW heterostructure repeatedly annealed at 800 °C. Anneal times are indicated on the figure. The fringe amplification is indicative of strains being developed within the specimen, with the well layer in tension at early stages of annealing, and in compression at later stages (see Fig. 4).

4800 s (80 min), a redshift has occurred in the PL data, and the corresponding 004 HRXRD is qualitatively ambiguous when referring to Fig. 4. Nevertheless, the lower fringe amplification is consistent with lower absolute strain values. The next data points at 8800 s (147 min) and 12 600 s (210 min) into the annealing are clearly consistent with an overall larger intermixing of group III atoms and a reversal of the strain sign; the well layer contains compressive strains and the barrier layers contain tensile strains. PL data are also consistent with a larger rate of diffusion of group III atoms beyond an annealing time of 4800 s.

The 004 rocking curves of Fig. 6 and their 002 counterparts were curve fitted as described in Sec. II B 3 to infer some quantitative measurements of strains and compositions. Fits were close, though not exact, and results could be refined with a more advanced version of the SMOOTHFIT software. These results nevertheless provide some information on the magnitude and location of strains in the sample, as well as the migration of arsenic and gallium away from the well center. Numerical results are given in Table I, and graphical results on strains and compositions are given, respectively, in Figs. 7 and 8.

An inversion of the strain fields has definitely occurred during annealing, as evidenced in Fig. 7. Figure 8 also supports a faster interdiffusion of group V material in the earlier stages of annealing, with the front of diffusion of phosphorus appearing to move faster towards the well center. A larger overall intermixing of group III material can be seen at the later stages of diffusion with the amount of gallium having been reduced by more than 50% of its original value in the well layer, while arsenic has been reduced by less than 40%.

Such a diffusion process was deemed possible by Cohen[17] under the influence of the miscibility gap. Supposing that group V diffusion is initially enhanced by the miscibility gap, he proposed that as the well compositions enter the latter, the associated increase of free energy from the positive enthalpy of mixing is initially compensated by the arsenic diffusion in the barrier layers, which itself lowers free energy by reducing the gradient of concentration on group V sublattice, until the total free energy in the system is no longer diminished. At this point, a radical diffusion of group III material is likely to occur, possibly through a spinodal type of decomposition of the alloys within the miscibility gap. The arrows in Fig. 9 crudely illustrate the process.

Also included in Fig. 9 are the dominant compositions presented in Table I for the well and barrier interdiffusion at 800 °C. The well compositions appear to follow closely the

TABLE I. Numerical values obtained from curve fitting 004 and 002 experimental rocking curves of a QW sample annealed at 800 °C. Data are presented graphically in Figs. 7 and 8. The "structure" column indicates the layer order from the substrate (S) and going upward to the capping layer (C).

Anneal time (C)	Layers	Composition	Thickness (nm)	Misfit (%)	Structure
315	W_1	$In_{0.531}Ga_{0.469}As$	1.79	0	
	W_2	$In_{0.531}Ga_{0.469}As_{0.912}P_{0.088}$	3.57	–0.293	$SBW_2W_1W_2BC$
	B	$In_{0.919}Ga_{0.081}As_{0.302}P_{0.698}$	2.78	0.405	
1000	W_1	$In_{0.531}Ga_{0.469}As$	0.50	0	
	W_2	$In_{0.531}Ga_{0.469}As_{0.885}P_{0.115}$	3.75	–0.384	$SBW_2W_1W_2BC$
	B	$In_{0.864}Ga_{0.136}As_{0.440}P_{0.560}$	3.31	0.470	
2400	W	$In_{0.531}Ga_{0.469}As_{0.860}P_{0.140}$	6.73	–0.450	SBWBC
	B	$In_{0.800}Ga_{0.200}As_{0.553}P_{0.453}$	3.80	0.392	
4800	W	$In_{0.580}Ga_{0.420}As_{0.832}P_{0.168}$	5.83	–0.220	
	B_1	$In_{0.781}Ga_{0.219}As_{0.576}P_{0.424}$	4.15	0.330	$SB_2B_1WB_1B_2C$
	B_2	$In_{0.941}Ga_{0.059}As_{0.058}P_{0.942}$	2.91	–0.234	
8800	W	$In_{0.727}Ga_{0.273}As_{0.700}P_{0.300}$	12.61	0.369	SBWBC
	B	$In_{0.909}Ga_{0.091}As_{0.090}P_{0.910}$	6.62	–0.354	
12 600	W	$In_{0.779}Ga_{0.221}As_{0.630}P_{0.370}$	13.32	0.496	SBWBC
	B	$In_{0.881}Ga_{0.119}As_{0.117}P_{0.883}$	6.90	–0.465	

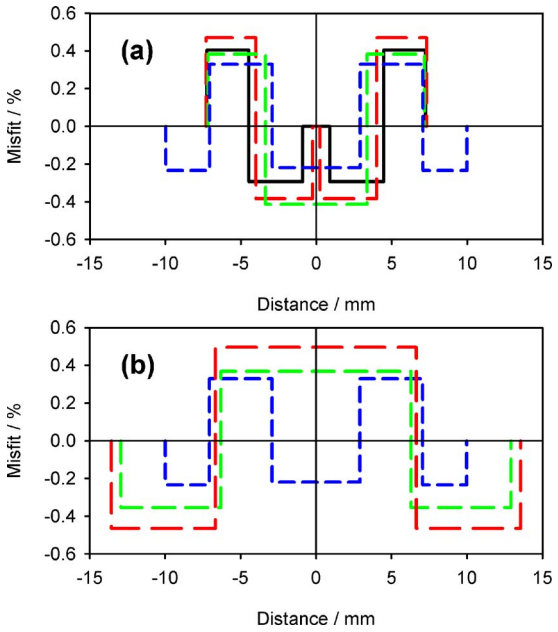

FIG. 7. (Color online) Strain profiles that generate a close fit to the experimental 004 rocking curves of Fig. 6. In (a) the solid line represents an anneal time of 315 s, the long dashes, 1000 s (red online), medium dashes, 2400 s (green online), and short dashes, 4800 s (blue online). In (b) the short dashes again show an anneal time of 4800 s (blue online), medium dashes, 8800 s (green online), and long dashes 12 600 s (red online). The top graph (a) shows strain fields consistent with a faster interdiffusion of group V atoms, with the well layer essentially in tension and the barrier layers containing compressive strains. A strain inversion starts occurring around an anneal time of 4800 s and the lower graph (b) shows strain fields consistent with a larger interdiffusion of group III atoms, with the well layer now in compression and the barrier layers containing tensile strains. The originally lattice matched well layer is 10 nm wide before annealing and centered on the abscissa origin.

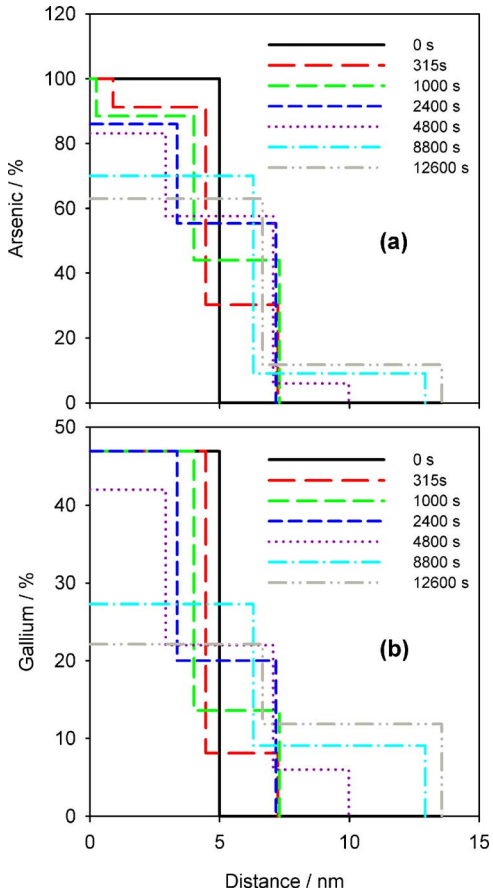

FIG. 8. (Color online) Composition profiles matching the strain profiles of Fig. 7 and also generating a close fit to the experimental 002 rocking curves measured on the same specimen repeatedly annealed at 800 °C; anneal times are indicated. (a) describes the alteration of the arsenic composition profile with anneal time, while (b) describes the gallium profiles. The abscissa origin is at the center of the well layer, profiles are symmetrical with respect to the well center, and only a half of the well layer is represented.

hypothesis proposed by Cohen, with diffusion probably occurring along a path around the miscibility gap. Further evidence of the responsibility of the miscibility gap for this diffusion process has already been published;[6] for lower anneal temperatures, the inversion in the PL shift occurs at an earlier stage of diffusion, and for higher anneal temperatures, no significant strains develop in annealed samples and interdiffusion appears to have identical rates for group III and V atoms. The temperature dependence of the diffusion process is consistent with a concomitant alteration of the extent of the miscibility gap in the quaternary diagram. A compositional jump occurs at 4800 s in the strained barrier layers with the onset of group III material diffusion. It is easy to see that should the average composition of the complete heterostructure lie within the miscibility gap, new layers with distinct alloy compositions and contrasting strains could be generated. Such layers generated by high temperature diffusion could prove to be stable against further thermal diffusion.

With the dependence of the diffusion path on temperature and compositions, and the variety of strain fields and compositions generated at various stages of annealing, it is not surprising that many results published in the literature appear at first contradictory. In a previous paper,[6] results were presented that showed very varied states of strains in originally lattice matched QW samples that were annealed at various temperatures for various lengths of time. Another source of confusion has been to rely on PL measurements alone and to use Fick's laws and a constant coefficient of diffusion to infer a state of diffusion in a sample. Clearly, values for activation energies and diffusion lengths derived from this model cannot be relied upon.

IV. CONCLUSION

HRXRD is a powerful tool that can provide accurate information on the composition distributions of interdiffused small heterostructures. A combination of PL and HRXRD measurements was used to characterize thermally induced interdiffusion in a lattice matched InGaAs/InP QW sample. A powerful methodology of characterization is proposed, whereby systematic HRXRD measurements are used to monitor thermal diffusion of QW structures. 004 rocking curves provide a means of characterization of the sample strain fields, and 002 curves are used to refine sample composition profile fits.

The diffusion process seems to follow a path around the miscibility gap, and further studies could be used as a means of experimentally surveying the latter at various temperatures with judicious choices of initial well and barrier com-

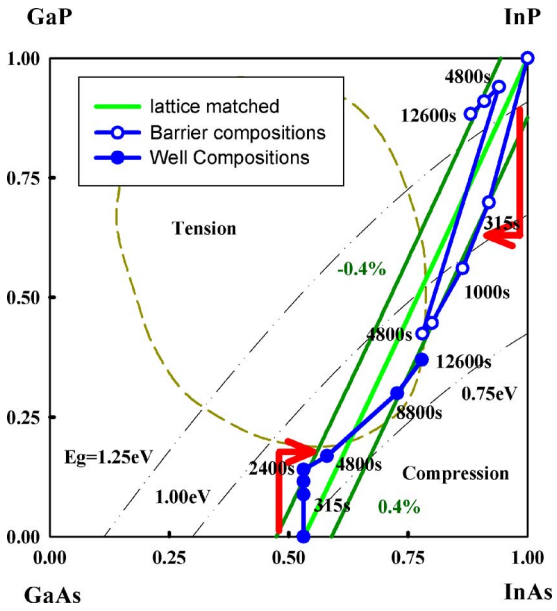

FIG. 9. (Color online) Quaternary diagram showing the line of lattice matched compositions to an InP substrate between two lines of compositions with an absolute misfit of 0.4%, some lines of constant band gap energy, and an approximation of the binodal isotherm calculated by Stringfellow (Ref. 9) at 677 °C. The compositions previously modeled (Fig. 8, Table I) are represented as circles with corresponding annealing times.

positions in QW samples. It should be noted that the miscibility gap appears to exist at higher temperatures than theoretically predicted so far.

During interdiffusion of originally lattice matched QW samples, layers of contrasting strains and compositions are generated. With an adequate choice of well/barrier thicknesses and compositions, alternated layers thus generated by thermal diffusion that would sit on opposite sides of the miscibility gap should prove to be compositionally stable against further heat exposure, while structurally providing the strengthening mechanisms associated with the coherently strained layers described in the Introduction.

[1]P. M. Anderson, T. Foecke, and P. M. Hazzledine, MRS Bull. **24**, 27 (1999).
[2]D. M. Dimiduk, P. M. Hazzledine, T. A. Parthasarathy, S. Seshagiri, and M. G. Mendiratta, Metall. Mater. Trans. A **29A**, 37 (1998).
[3]M. E. Brenchley, M. Hopkinson, A. Kelly, P. Kidd, and D. J. Dunstan, Phys. Rev. Lett. **78**, 3912 (1997).
[4]N. B. Jayaweera, A. J. Bushby, A. Kidd, A. Kelly, and D. J. Dunstan, Philos. Mag. Lett. **79**, 343 (1999).
[5]F. Bollet, W. P. Gillin, M. Hopkinson, and R. Gwilliam, J. Appl. Phys. **93**, 3881 (2003).
[6]F. Bollet and W. P. Gillin, J. Appl. Phys. **94**, 988 (2003).
[7]F. Bollet, W. P. Gillin, M. Hopkinson, and R. Gwilliam, J. Appl. Phys. **97**, 013536 (2005).
[8]B. De Cremoux, P. Hirtz, and J. Ricciardi, *Proceedings of the 1980 International Symposium on GaAs and Related Compounds* (The Institute of Physics, Oiso, Japan, 1981), vol. 56, p. 115.
[9]G. B. Stringfellow, J. Cryst. Growth **58**, 194 (1982).
[10]K. Onabe, Jpn. J. Appl. Phys., Part 1 **21**, 797 (1982).
[11]G. B. Stringfellow, J. Cryst. Growth **65**, 454 (1983).
[12]D. Schlenker *et al.*, Jpn. J. Appl. Phys., Part 1 **39**, 5751 (2000).
[13]L. V. Azároff, R. Kaplow, N. Kato, R. J. Weiss, A. J. C. Wilson, and R. A. Young, *X-Ray Diffraction* (McGraw-Hill, New York, 1974).
[14]C. Bocchi and C. Ferrari, J. Phys. D **28**, A164 (1995).
[15]P. F. Fewster, Semicond. Sci. Technol. **8**, 1915 (1993).
[16]P. F. Fewster, Rep. Prog. Phys. **59**, 1339 (1996).
[17]R. M. Cohen, J. Appl. Phys. **73**, 4903 (1993).